Erschienen in: Soft Matter ; 17 (2021), 10
https://dx.doi.org/10.1039/d0sm02021d

Critical Casimir interactions of colloids in micellar critical solutions

Laurent Helden, *[a] Timo Knippenberg,[b] Li Tian,[b] Aubin Archambault,[b] Felix Ginot[b] and Clemens Bechinger[b]

We study the temperature-dependence of critical Casimir interactions in a critical micellar solution of the nonionic surfactant $C_{12}E_5$ dissolved in water. Experimentally, this is achieved with total internal reflection microscopy (TIRM) which measures the interaction between a single particle and a flat wall. For comparison, we also studied the pair interactions of a two dimensional layer of colloidal particles in the identical micellar system which yields good agreement with the TIRM results. Although, at the surfactant concentration considered here, the fluid forms a dynamical network of wormlike micelles whose structure is considerably more complex than that of simple critical molecular fluids, the temperature-dependence of the measured interactions is – for surface-to-surface distances above 160 nm – in excellent quantitative agreement with theory. Below 160 nm, deviations arise which we attribute to the adsorption of micelles to the interacting surfaces.

Introduction

Critical Casimir forces have received considerable attention as a versatile interaction in soft matter systems which can be precisely and fully reversibly controlled by smaller variations in temperature.[1–4] They arise due to the spatial confinement of critical concentration fluctuations in the fluid which diverge upon approaching the critical point. Depending on boundary conditions, *i.e.* whether the two confining surfaces prefer the same or the opposite component of the mixture, forces can be attractive or repulsive, respectively. Because of the universal properties of critical points, critical Casimir forces are expected to arise in a wide range of systems near their critical point. While most experiments have been conducted in molecular binary mixtures,[2,3,5] several studies exist using aqueous mixtures of nonionic surfactants.[1,6] The latter are particularly interesting because they promise much larger interaction ranges of critical Casimir forces due to their larger correlation lengths. Owing to their mesoscopic micellar structure, however, it is not immediately obvious whether critical Casimir forces are superimposed by other types of interactions, *e.g.*, entropic forces. These entropic forces can be depletion interactions[7] and other excluded volume effects due to the flexibility of the micelles.[8]

Here we study critical Casimir forces in an aqueous critical solution of the nonionic surfactant $C_{12}E_5$. The surfactant belongs to the widespread class of polyoxyethylene alkyl ether (C_nE_m) having applications in drug delivery systems, cosmetic formulations and cleaning detergents.[9] Opposed to molecular solvents, such systems – at the concentrations relevant for our study – typically form complex networks which are characterized by several mesoscopic length scales as can be seen in cryo-TEM images.[10] In case of $C_{12}E_5$, light scattering experiments demonstrate the presence of wormlike micelles of 2.2 nm diameter.[11,12] While the diameter is rather insensitive to the temperature and surfactant concentration, the contour length of the wormlike micelles varies between 300 nm and 1400 nm at the critical concentration and a temperature range ($20\ ^\circ C \lesssim T \lesssim 31\ ^\circ C$) comparable to that of our study. Because of the low stiffness[11,12] of these wormlike micelles the network is rather flexible and thus strongly susceptible to thermal fluctuations. Given such a complex and dynamical internal structure, however, it is not clear how this affects critical Casimir forces in such systems.

Experimental

$C_{12}E_5$ is strongly hygroscopic, therefore the aqueous mixture has been prepared within a glove box in absence of humidity. At a lower surfactant concentration (being above the critical micellar concentration), $C_{12}E_5$ mixtures separate into a concentrated and dilute micellar solution. The corresponding lower critical point is located at 1.2 wt% $C_{12}E_5$ and $T = T_C \approx 32\ ^\circ C$, see *e.g.* ref. 11 and 13 for a full phase diagram. Critical Casimir interactions between a single colloidal probe particle

[a] *2. Physikalisches Institut, Universität Stuttgart, Pfaffenwaldring 57, Stuttgart, D-70550, Germany. E-mail: L.Helden@pi2.uni-stuttgart.de*
[b] *Fachbereich Physik, Universität Konstanz, Konstanz, D-78464, Germany*

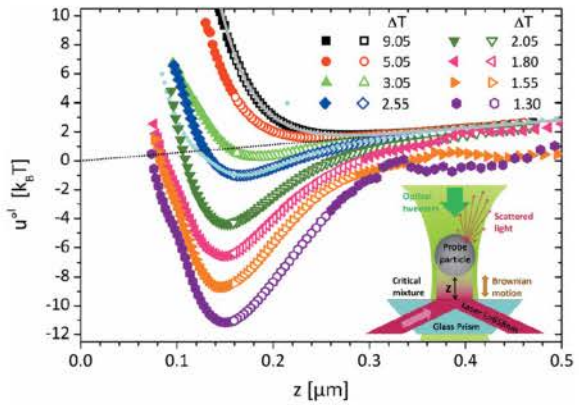

Fig. 1 Temperature-dependent interaction potentials between a PS sphere and a flat silica substrate in a critical $C_{12}E_5$ solution measured with TIRM (filled and open symbols). ΔT values, *i.e.*, the deviation from critical temperature, are given in the legend. The solid line (grey) on top of the squares (black) corresponds to a fit to $u^{\circ|}_{el} + u^{\circ|}_{ext}$. The dotted straight line (black) represents $u^{\circ|}_{ext}$. Experimental values represented by open symbols are fitted in Fig. 2. The inset depicts a sketch of the TIRM experiment.

and a silica wall in such a critical mixture have been measured using total internal reflection microscopy (TIRM).[14,15] A laser beam is totally internally reflected at the interface between a glass prism and the critical mixture leading to an evanescent field penetrating the fluid (see Fig. 1 inset). From the light intensity, scattered from the evanescent field by a single colloidal probe particle, the particle–wall distance probability distribution $P(z)$ can be obtained. Under equilibrium conditions, this finally yields the particle–wall interaction potential $u^{\circ|}(z)$ using the Boltzmann probability distribution. To avoid particle diffusion out of the field of view, its lateral motion is confined by an optical tweezers.[16] The temperature stability of the sample cell and during typical data acquisition time scales ($\frac{1}{2}$ to 2 h) is ± 10 mK. As a probe particle we used a polystyrene (PS) particle with $a = 1.25$ μm radius and sulfate surface groups rendering it hydrophilic and negatively charged. The same conditions apply to the glass prism. This leads to an electrostatic repulsion at short distances. To study the lateral interaction between colloidal particles, we also employed video microscopy and particle tracking.

Results and discussion

Particle wall interactions

Fig. 1 shows the distance-dependent interaction potentials as a function of the temperature obtained with TIRM. Far below the critical temperature ($\Delta T = T_C - T = 9.05$ K, black squares) no attractive Casimir forces are present and the particle wall interaction is entirely repulsive. At larger distances, the potential exhibits a linear attractive part which is due to gravity and optical forces.[16] Gravitational and optical forces are summarized as F_{ext} and give rise to a linear potential $u^{\circ|}_{ext} = F_{ext} z$ which is shown as dotted straight line (black) in Fig. 1.

The electrostatic interaction is given by $u^{\circ|}_{el} = B\exp\{-z/\lambda_D\}$, where λ_D is the Debye screening length and B a factor depending on the surface charges of the particle and the wall.[14,15,17] It can be assumed that the electrostatic repulsion is essentially unaffected by the non-ionic surfactant. Best agreement with our data is obtained with $\lambda_D = 33.4$ nm. This value corresponds to an ionic concentration of 83 μM of monovalent salt and is probably caused by residual impurities or dissolved CO_2 in our solution. When further approaching T_C, an increasingly attractive component in the potential appears, which causes a shift of the potential minima towards smaller distances (Fig. 1).

While the potentials obtained at $z > 160$ nm are highly reproducible, this is not the case for smaller distances. Below 160 nm, variations between experiments which have been conducted at identical conditions were observed. This is exemplarily shown for two measurements at $\Delta T = 2.55$ K (large and small diamonds) which were taken with a time interval of 7 h. It appears as additional attraction increasing up to several k_BT for smaller distances in the data for small diamonds compared to the large diamonds. Similar variations at $z \lesssim 160$ nm occur also for other temperatures and are unsystematic *i.e.* they neither grow nor vanish monotonously with time. We attribute this behavior to the adsorption of globules and rods of the surfactant which has been reported to occur on silica surfaces.[18] Due to the high flexibility of such structures, this may explain the observed temporal variations of the interaction potential at small distances. In the following, we have therefore restricted our data analysis to the range $z > 160$ nm. Furthermore, data with poor statistics (<1000 counts in the probability distribution histogram) appearing *e.g.* at larger distances was neglected. To extract the temperature-dependent critical Casimir contribution from the potentials, in the following we have subtracted $u^{\circ|}_{el}$ and $u^{\circ|}_{ext}$ from our data (open symbols in Fig. 2).

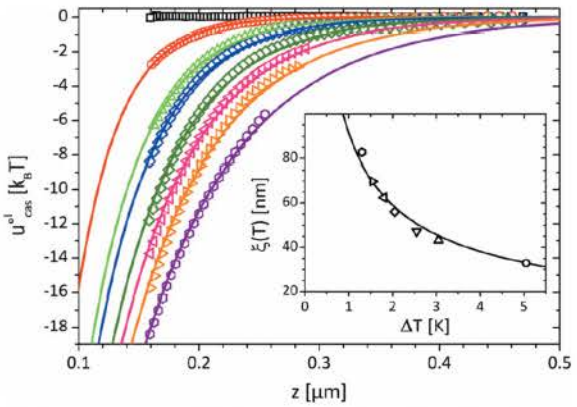

Fig. 2 Interaction potentials from Fig. 1 after subtraction of $u^{\circ|}_{el} + u^{\circ|}_{ext}$ (symbols in correspondence to Fig. 1). Solid lines correspond to fits of eqn (1) with the correlation length ξ as the only fitting parameter. The inset shows the obtained values of ξ as a function of temperature (symbols) with the solid line a fit to eqn (2).

Theoretically, the critical Casimir interaction between a sphere and a flat wall is given by[3,19]

$$u^{\circ|}_{cas}(z) = k_B T \frac{a}{z} \vartheta^{\circ|}(z/\xi), \quad (1)$$

with $\vartheta^{\circ|}(z/\xi)$ the universal scaling function for symmetric boundary conditions and infinitely strong surface fields.[19,20] The temperature-dependent correlation length is

$$\xi(T) = \xi_0(\Delta T/T_C)^{-\nu} \quad (2)$$

with the three-dimensional Ising exponent $\nu = 0.63$ and ξ_0 a characteristic microscopic length scale.[21] The solid lines in Fig. 2 are fits to eqn (1) with ξ used as the only free parameter and show excellent agreement with the data. As shown by the inset of Fig. 2, indeed the obtained values of $\xi(T)$ follow the temperature dependence predicted by eqn (2). From this, the prefactor for the $C_{12}E_5$ micellar solution is determined to $\xi_0 = 2.5 \pm 0.1$ nm. This value is within the range of values estimated by light scattering for $C_{12}E_5$ solutions.[21,22] Notably, it is very close to the micellar diameter of 2.2 nm being indeed the smallest relevant length scale of the system.[11,12] Because the diameter is rather independent of temperature (in contrast to the contour length of the wormlike micelles) this might explain why ξ_0 adopts this length scale.

Particle particle interactions

In addition to the above experiments with a single particle near a flat wall, we also performed critical Casimir pair potential $u(r)$ measurements between colloidal particles which additionally interact with an underlying substrate. The experiments were carried out in a thin silica capillary which is sealed with epoxy glue and was filled with a critical micellar solution of water and $C_{12}E_5$. As colloidal particles we have used spherical silica particles with radius $a = 1.2$ μm and a silanol surface functionalization, rendering them negatively charged. They form a quasi-two-dimensional layer at the bottom plate due to gravitational forces (gravitational length $\approx$ 30 nm). Because critical Casimir forces are not sensitive to the bulk material but only depend on the surface adsorption properties, the hydrophilic silica particles are expected to lead to identical results as those of the hydrophilic PS particles used in the TIRM experiments.[23]

Fig. 3(a–c) show typical particle configurations at $\Delta T = 9$ K, 5 K, and 3 K, respectively, demonstrating the strong temperature dependence of such interactions on the configuration of a colloidal monolayer. Typical experiments were performed at particle densities of about 0.03 μm^{-2} and for about 60 minutes where snapshots are taken with a rate of 3 fps. Prior to each measurement, the sample was allowed to equilibrate for about 45 min to avoid thermal gradients after changing the bath temperature. Note, that for $\Delta T = 3$ K, the attraction is already so large, that clusters do not dissolve during experimental time scales (compare Fig. 3c). Under such conditions, no pair potentials can be obtained from configurational data.

Fig. 3 Snapshots of equilibrated configurations of a semidilute two-dimensional suspension of colloidal silica particles with radius $a = 1.2$ μm in a critical micellar solution at different temperatures as indicated.

In case of micron-sized particles, whose positions are immediately accessible with optical microscopy, pair interactions are easily obtained. At dilute particle concentrations, the potential of mean force which is immediately derived from the pair correlation function $g(r)$ becomes identical with the pair interaction $u(r)$.[24] In case of short-ranged interactions and slow particle dynamics (either because of a large particle size or a high solvent viscosity), however, this approach may require long experimental time scales to guarantee the sampling of sufficient amount of configurationally independent data. To overcome such problems, we have followed a recently proposed method which avoids such difficulties because it allows to measure pair interactions at densities much higher than the dilute limit.[25] Compared to other methods which require *a priori* information regarding the interactions in the system,[26–29] this approach is entirely model-free.

Insertion method

The insertion method developed by Stones *et al.*[25] uses the pair correlation function $g(r)$ to indirectly measure the pair potential $u(r)$. The idea is to first compute the pair correlation function $g_{ref}(r)$ with the traditional "histogram" method (*i.e.* by measuring the histogram of distances between particles, and normalizing it). This reference measurement is then compared with a test measurement $g_i(r)$, obtained through the insertion of fictitious particles with a hypothetical pair interaction $u_i(r)$.

$$g_i(r) = \frac{\langle \exp\{-\Psi/k_B T\}_r \rangle}{\langle \exp\{-\Psi/k_B T\} \rangle} \quad (3)$$

with $\Psi = \sum u_i(r')$ and k_B the Boltzmann constant. Here Ψ corresponds to the energy cost of inserting a fictitious particle at a distance r of a real particle. It is calculated using the sum of pairwise interactions $u_i(r')$ between the fictitious particle and the surrounding real particles at distance r'. The pair potential is then updated using:

$$u_{i+1}(r) = u_i(r) + k_B T \ln\left(\frac{g_i(r)}{g_{ref}(r)}\right) \quad (4)$$

Through this predictor–corrector process, one can update the value of $u_i(r)$ step by step, until the insertion measurement $g_i(r)$ matches the reference $g_{ref}(r)$. As $g(r)$ is unique at equilibrium, this happens when $u_i(r) \simeq u(r)$. As already mentioned, a key benefit of this method is that it allows to measure the exact pair interaction, even for dense systems (no dilute limit hypothesis).

Interaction potentials

Fig. 4a shows the temperature-dependent measured pair correlation functions. With increasing temperature, one observes a pronounced increase of the first peak which also shifts to

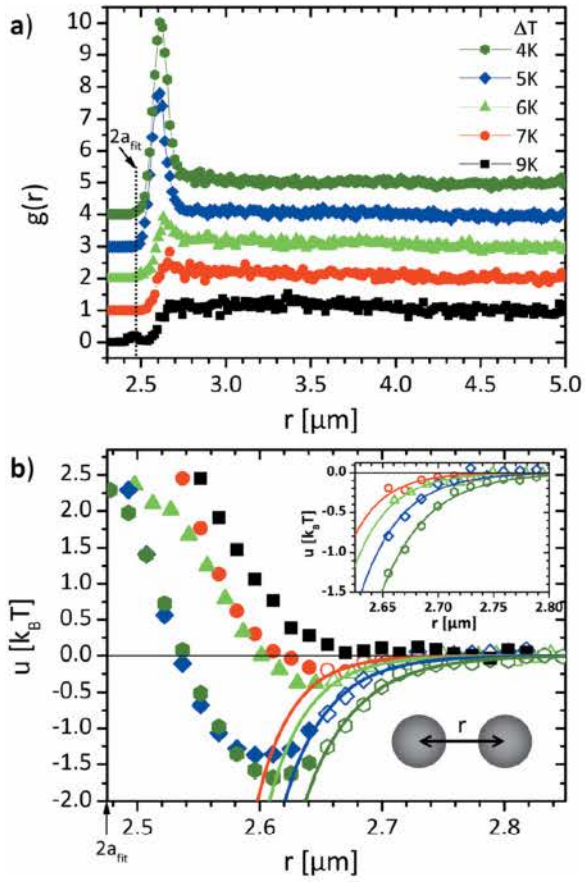

Fig. 4 (a) Experimentally measured temperature-dependent pair correlation functions (to avoid data overlap, the curves are vertically shifted by one unit relative to each other). ΔT values are given in the legend. (b) Derived temperature-dependent pair interaction potentials from experimental data (filled and open symbols). The solid lines correspond to a parameter-free calculation of critical Casimir forces. The inset shows a zoom into the data. Data displayed as open symbols was used to fit the radius a_{fit}.

smaller distances. This is in qualitative agreement with the presence of attractive critical Casimir forces which increase upon approaching the critical temperature. The corresponding pair interactions $u(r)$ derived from the method described above are shown in Fig. 4b. In addition to an attractive strongly temperature-dependent component, particle repulsion is observed at small distances due to the negative surface charges of the particles. This is qualitatively the same behavior as observed for the particle wall interactions (compare Fig. 1).

To compare the measured critical Casimir potentials between a sphere and a flat wall obtained by TIRM (Fig. 2) with the corresponding critical Casimir pair interaction as shown in Fig. 4, the scaling function has to be adjusted. Within the Derjaguin approximation this leads to[19]

$$u_{cas}(r) = k_B T \frac{a}{2(r-2a)} \vartheta^{\circ|}\left(\frac{r-2a}{\xi}\right). \quad (5)$$

The corresponding results calculated using the parameter ξ_0 determined in the TIRM experiments are shown as solid lines in Fig. 4b. The only adjustable parameter in the fit was the particle radius a. Similar to the TIRM data analysis, small surface distances (dominated by electrostatics and adsorption effects) have been neglected for the fit (see Fig. 4b inset). Best agreement with the data was found for $a_{fit} = 1.23 \pm 0.02$ μm which is close to the nominal particle radius of 1.20 μm.

Clearly, the agreement between the experimental data in Fig. 4b with theory is less accurate than those obtained from the TIRM measurements (Fig. 2). At first glance this may be a result of three-body critical Casimir interactions which indeed have been observed.[30] Such contributions, however, are – for comparable correlation lengths achieved by us – restricted to surface distances below 100 nm. In addition, at the particle concentrations considered here, closely packed trimers form only rarely. In fact, the larger deviations of the pair potentials obtained using eqn (3) are attributed to the finite polydispersity (around 2%) which is not considered in this method[26] and naturally is no issue in TIRM experiments where a single probe in front of a wall is considered.

Discussion of measured interactions

While the measured interactions in sphere–wall and sphere–sphere geometry both agree well with the theoretical predictions for critical Casimir forces, it is at a first glance surprising, not to find any signs of depletion forces in our system. The latter have been observed in the very similar $C_{12}E_6$ micellar system.[7] Here Grattle *et al.* observed temperature dependent attractive potentials of up to $2k_BT$ in the temperature range from 22–28 °C in a system containing 44 mM $C_{12}E_6$ and 17 mM NaCl. However, it should be noted, that those experiments have been performed in the presence of salt ($\lambda_D = 2.3$ nm), which renders the micelles negatively charged, largely increasing its efficiency as a depletion agent.[31]

Still for our uncharged system depletion forces are expected and the range of interactions typically coincides with the size of the depletion agent (*e.g.* diameter or length). Thus, in our system, the wormlike micelles of a few 100 nm couture length could induce depletion forces in the same distance range where critical Casimir forces were observed in this study. Furthermore, the temperature dependent contour length could lead to an additional temperature dependent interaction. Since this is not observed in the distance range, where we fitted the critical Casimir forces, we conclude that the high flexibility of the wormlike micelles, having a temperature independent stiffness parameter of only $\lambda^{-1} = 12$ to 25 nm[12] substantially reduces the range of depletion interaction. Probably the range of depletion forces is rather set by λ^{-1} than the length, which would be the appropriate parameter for rigid depletion agents.[32]

Thus, in our experiments depletion forces are "hidden" by the electrostatic repulsion, dominant for these small distances. Possibly the variations for $z < 160$ nm, discussed in the context of Fig. 1, have their origin in some entropic interactions.

The fact that the temperature dependent attractive forces, that we attribute to critical Casimir interactions decay within

the theoretically expected temperature range is a further proof of the absence of depletion forces, because the latter are known to persist down to temperatures much further below $T_C \approx 52\ ^\circ C$[12] for the $C_{12}E_6$ system employed by Gratale *et al.*[7]

Conclusions

In summary, we have measured attractive critical Casimir pair interactions in a critical micellar aqueous solution of the nonionic surfactant $C_{12}E_5$. Although such systems form a complex and dynamical wormlike micellar network near the critical point, the measured temperature-dependence of the interaction potentials are in excellent agreement with theory over a wide range of surface-to-surface distances. The prefactor of the correlation length is set by the diameter of the wormlike micelles which is known to hardly vary with temperature. Only at surface distances below $z \approx 160$ nm, deviations are observed which are attributed to the presence of adsorption layers on the interacting surfaces.

Compared to other molecular critical solvents, micellar systems offer the advantage of potentially much larger correlation lengths leading to larger interaction ranges. In addition, critical aqueous mixtures are chemically less aggressive compared *e.g.*, to frequently used water–lutidine mixtures and thus provide larger flexibility regarding the materials used for sample preparation.

Conflicts of interest

The authors do not have any conflicts to declare.

Acknowledgements

We acknowledge helpful discussions with D. Aarts and R. Piazza. The project is supported by the Deutsche Forschungs-gemeinschaft *via* the Collaborative Research Center 1214.

Notes and references

1 I. Martínez, C. Devailly, A. Petrosyan and S. Ciliberto, *Entropy*, 2017, **19**, 77.
2 V. D. Nguyen, S. Faber, Z. Hu, G. H. Wegdam and P. Schall, *Nat. Commun.*, 2013, **4**, 1584.
3 C. Hertlein, L. Helden, A. Gambassi, S. Dietrich and C. Bechinger, *Nature*, 2008, **451**, 172–175.
4 M. E. Fisher and P.-G. de Gennes, *Simple Views on Condensed Matter*, 2003, pp. 237–241.
5 D. Beysens and D. Estève, *Phys. Rev. Lett.*, 1985, **54**, 2123–2126.
6 S. Buzzaccaro, J. Colombo, A. Parola and R. Piazza, *Phys. Rev. Lett.*, 2010, **105**, 198301.
7 M. D. Gratale, T. Still, C. Matyas, Z. S. Davidson, S. Lobel, P. J. Collings and A. G. Yodh, *Phys. Rev. E*, 2016, **93**, 050601(R).
8 Y. Suganuma, N. Urakami, R. Mawatari, S. Komura, K. Nakaya-Yaegashi and M. Imai, *J. Chem. Phys.*, 2008, **129**, 134903.
9 F. N. Padia, M. Yaseen, B. Gore, S. Rogers, G. Bell and J. R. Lu, *J. Phys. Chem. B*, 2014, **118**, 179–188.
10 A. Bernheim-Groswasser, E. Wachtel and Y. Talmon, *Langmuir*, 2000, **16**, 4131–4140.
11 Y. Einaga, *Polym. J.*, 2009, **41**, 157–173.
12 S. Shirai and Y. Einaga, *Polym. J.*, 2005, **37**, 913–924.
13 R. Strey, R. Schomäcker, D. Roux, F. Nallet and U. Olsson, *J. Chem. Soc., Faraday Trans.*, 1990, **86**, 2253–2261.
14 D. C. Prieve, *Adv. Colloid Interface Sci.*, 1999, **82**, 93–125.
15 J. Y. Walz, *Curr. Opin. Colloid Interface Sci.*, 1997, **2**, 600–606.
16 J. Y. Walz and D. C. Prieve, *Langmuir*, 1992, **8**, 3073–3082.
17 H. H. v. Grünberg, H. H. von Grünberg, L. Helden, P. Leiderer and C. Bechinger, *J. Chem. Phys.*, 2001, **114**, 10094–10104.
18 A. Blom, G. G. Warr and E. J. Wanless, *Langmuir*, 2005, **21**, 11850–11855.
19 A. Gambassi, A. Maciołek, C. Hertlein, U. Nellen, L. Helden, C. Bechinger and S. Dietrich, *Phys. Rev. E: Stat., Nonlinear, Soft Matter Phys.*, 2009, **80**, 061143.
20 O. Vasilyev, A. Gambassi, A. Maciołek and S. Dietrich, *EPL*, 2007, **80**, 60009.
21 G. Dietler and D. S. Cannell, *Phys. Rev. Lett.*, 1988, **60**, 1852–1855.
22 J. P. Wilcoxon, *J. Phys. Chem.*, 1990, **94**, 7588–7596.
23 U. Nellen, L. Helden and C. Bechinger, *EPL*, 2009, **88**, 26001.
24 D. Chandler and J. K. Percus, *Phys. Today*, 1988, **41**, 114–118.
25 A. E. Stones, R. P. A. Dullens and D. G. A. L. Aarts, *Phys. Rev. Lett.*, 2019, **123**, 098002.
26 T. O. Pangburn and M. A. Bevan, *J. Chem. Phys.*, 2005, **123**, 174904.
27 M. Brunner, C. Bechinger, W. Strepp, V. Lobaskin and H. H. von Grünberg, *EPL*, 2002, **58**, 926–965.
28 S. H. Behrens and D. G. Grier, *Phys. Rev. E*, 2001, **64**, 050401(R).
29 M. D. Carbajal-Tinoco, F. Castro-Román and J. L. Arauz-Lara, *Phys. Rev. E: Stat., Nonlinear, Soft Matter Phys.*, 1996, **53**, 3745–3749.
30 S. Paladugu, A. Callegari, Y. Tuna, L. Barth, S. Dietrich, A. Gambassi and G. Volpe, *Nat. Commun.*, 2016, **7**, 11403.
31 D. L. Sober and J. Y. Walz, *Langmuir*, 1995, **11**, 2352–2356.
32 L. Helden, R. Roth, G. H. Koenderink, P. Leiderer and C. Bechinger, *Phys. Rev. Lett.*, 2003, **90**, 048301.